GUO. M., PARADA, S., SMETS, S., JONES, P.T., VAN DYCK, J. BLANPAIN, B., and WOLLANTS, P. Laboratory study of the interaction mechanisms between magnesia-chromite refractories and Al_2O_3-rich VOD slags. *VII International Conference on Molten Slags Fluxes and Salts,* The South African Institute of Mining and Metallurgy, 2004.

Laboratory study of the interaction mechanisms between magnesia-chromite refractories and Al_2O_3-rich VOD slags

M. GUO, S. PARADA, S. SMETS, P.T. JONES, J. VAN DYCK, B. BLANPAIN, and P. WOLLANTS
Department of Metallurgy and Materials Engineering, Katholieke Universiteit Leuven, Heverlee, Belgium

The corrosion behaviour of a high-quality rebonded magnesia-chromite refractory in contact with a vacuum oxygen decarburization (VOD) slag with high Al_2O_3 content (15–20 mass per cent) is investigated under VOD process conditions by rotating finger tests in a vacuum induction furnace. The refractory degradation mechanisms are studied by the characterization of corroded microstructures using scanning electron microscopy, equipped with energy dispersive spectroscopy. The influence on the refractory wear of the process temperature and the Al_2O_3 content in the slag is discussed.

Keywords: corrosion, magnesia-chromite refractory, VOD slags, vacuum induction furnace

Introduction

The vacuum oxygen decarburisation (VOD) is a secondary refining step for the production of stainless steel. During the VOD reduction stage, Cr_2O_3 is recovered from the slag through additions of ferrosilicon and/or aluminium. Moreover, these alloys are often added as supplementary fuel to obtain sufficiently high temperatures for continuous casting. VOD reduction slags thus consist of CaO, MgO, Al_2O_3 and SiO_2 as major components, together with smaller quantities of Cr_2O_3 and minor amounts of MnO, TiO_2 and FeO_x. Elevated Al_2O_3 levels in the slag increase the lime solubility and sulphide capacity of the slag. From a metallurgical point of view, Al_2O_3-rich CaO-SiO_2-MgO-Al_2O_3 (CSMA) slags would be beneficial to the desulphurization process.

Due to the harsh conditions imposed by the VOD process on the refractory lining, a sound material selection is of paramount importance. Magnesia-chromite bricks are widely applied in the slaglines of VOD ladles because of their excellent slag resistance, dimensional stability and high hot-temperature strength. A multitude of studies concerning the wear mechanisms of this refractory class and the influence of slag compositions has been published.[1–11] Jones *et al.*[1–3] investigated the degradation mechanisms of magnesia-chromite bricks in VOD applications by post-mortem assessment of industrially worn specimens, corroded by Al_2O_3-poor CSMA slags (< 8 mass per cent Al_2O_3). Similarly, Mosser *et al.*[4] observed that the magnesia-chromite refractories in Reinstahl Heraeus (RH) degassing units suffer from the infiltration of silica-rich or alumina-containing slag into the pores, reaction of the infiltrated slag with the brick matrix, and the subsequent hot erosion of the infiltrated zone.

Some specific studies on the influence of basicity on magnesia-chromite wear are also available. Calkins *et al.*[5] exposed direct-bonded magnesia-chromite refractories to different slags and found that chromite was more resistant than periclase in an acid slag ($CaO/SiO_2 = 0.5$), while periclase was more resistant in basic slags ($CaO/SiO_2 = 2$). Narita *et al.*[6] confirmed that the corrosion of magnesia-chromite refractories increased with decreasing slag basicity, expressing the latter as:

$$B_{\text{basic slag}} = \left[(CaO + MgO)/(SiO_2 + Al_2O_3)\right] \quad [1]$$

with MO_x in mass per cent. However, Al_2O_3 often plays an ambiguous role: in acidic slags it can also behave basic, thus affecting basicity in a CSMA slag as follows:[12]

$$B_{\text{acid slag}} = \left[(CaO + MgO + Al_2O_3)/(SiO_2)\right] \quad [2]$$

Al_2O_3 then acts as a fluxing component, thus enhancing slag fluidity and thereby also the infiltration into the refractory material. On the other hand, it also reduces the MgO solubility in the slag, therefore decreasing periclase dissolution. The Al_2O_3 content thus clearly influences the corrosion mechanisms of magnesia based refractories.

However, there are few systematic studies available on the effect of Al_2O_3-rich CSMA VOD slags—which could be interesting for metallurgical reasons—on the degradation mechanisms of magnesia-chromite refractories under VOD process conditions. In the present paper, the corrosion behaviour of a magnesia-chromite brick in contact with a VOD slag with high Al_2O_3 content (15–20 mass per cent) is therefore investigated. This is done through rotating finger tests in a vacuum induction furnace simulating VOD process conditions. The refractory degradation mechanisms are studied by the characterization of corroded microstructures using scanning electron microscopy (SEM), equipped with energy dispersive spectroscopy (EDS). The influence of temperature and Al_2O_3 content on the refractory corrosion is discussed.

Experimental

Experimental approach and parameters

Rotating finger tests were performed with a vacuum induction furnace (type VSG 30, 60 kW power supply, 4 kHz frequency). Cylindrical refractory specimens (28×200 mm) were dipped into the corrosive slag and liquid stainless steel, and rotated for a certain numbering of cycles (rotation speed: 12 rpm). A schematic diagram of the experimental

set-up is shown in Figure 1a. The experimental conditions are listed in Table I. An Al_2O_3 crucible (175×220 mm) was used in the present tests, resulting in high Al_2O_3 content slags. Approximately 15 kg of stainless steel (AISI 316), 2.6 kg of VOD-reduction slags (Table II) supplied by a stainless steel company and a commercially available top-quality rebonded magnesia-chromite refractory material (density: 3.38 g/cm^3, open porosity: 12 volume per cent) were employed in the tests. In order to simulate the atmosphere in the VOD process, a gas mixture of CO and CO_2 was blown into the furnace at flow rates of 50 l/min CO and 1 l/min CO_2, controlled by mass-flow meters. The oxygen partial pressure was thus set to be ~10^{-11} atm. Three tests were carried out at distinct temperatures (Test 1 and Test 2: 1600°C; Test 3: 1670°C) and exposure times of 60, 120 and 240 min, respectively.

Experimental procedure

After charging the stainless steel in the Al_2O_3 crucible, the furnace was evacuated down to approximately 5 mbar. The steel was then heated to the experimental temperature by slowly increasing the furnace power in its 'manual mode'. Heating was commenced at a power level of 5 kW, after which the power was increased by 2.5 kW every 10 minutes until the metal had melted completely. Subsequently, the slag was added to the metal through the loading chamber. After the slag was in a fully liquid state, the temperature was regulated to the expected value by means of changing the power according to the experimentally determined power-temperature curve. The latter has been described in previous work by the present authors.[13] Thereafter, the temperature of the melt was measured by a dip thermocouple (type B: Pt 30%Rh/Pt 6%Rh). For the sake of

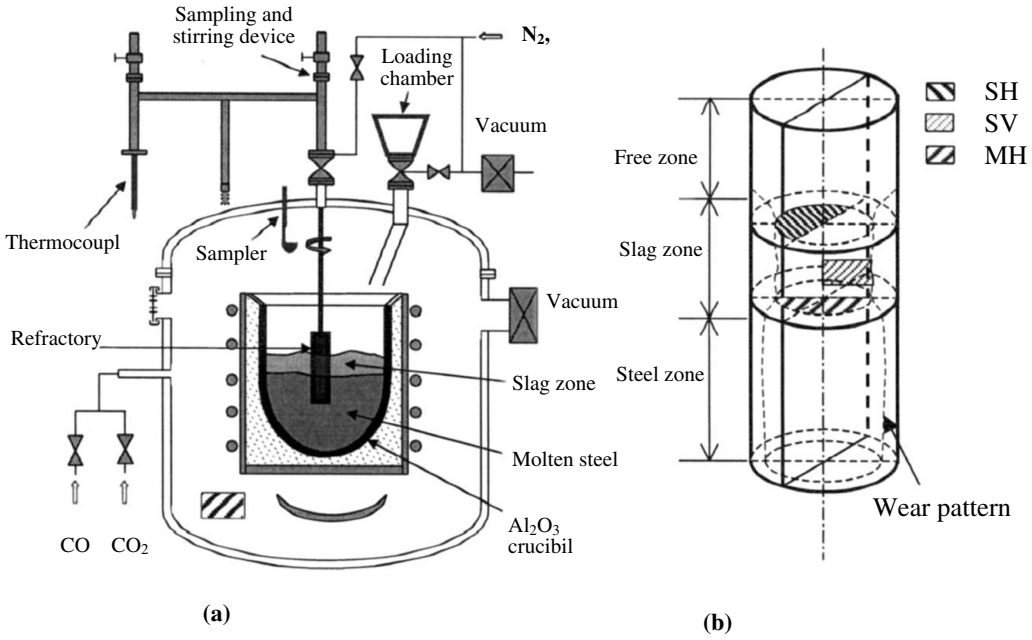

Figure 1. Schematic diagram of the experimental set-up, showing (a) Rotating finger test, (b) Sample extraction scheme

Table I
Experimental parameters

Exp. No.	Time (min)	Temp. (°C)	P_{O_2} (atm)	Refractory materials	Other parameters
Test 1	60	1600	1.72×10^{-11}	Rebonded Magnesia-chromite	Steel amount: 15 kg Slag amount: 2.6 kg Rotating speed: 12 rpm Pressure: 5 mbar Sample size: ϕ28 × 200 mm
Test 2	120	1600	7.01×10^{-11}		
Test 3	240	1670	7.20×10^{-11}		

Table II
Chemical composition of the (as-delivered) VOD slag initially charged in the experiments (mass%), as determined by ICP-AES

	MgO	Cr_2O_3	Al_2O_3	FeO	CaO	SiO_2	MnO	TiO_2
1	13.1	8.7	1.2	1.4	29	45	1.5	< 0.5
2	13.5	8.0	2.6	0.8	27	44	2.1	< 0.5
3	13.0	7.7	1.5	1.3	28	45	1.9	< 0.5
Average	**13.2**	**8.1**	**1.8**	**1.1**	**28**	**45**	**1.8**	**< 0.5**

temperature stabilization and to obtain high Al_2O_3 content in the slags, it was held for 40 min at the same power setting. After this period, the temperature was measured once more. Due to the fact that the temperature difference between two consecutive measurements was less than 5°C, we considered the temperature as stable. Subsequently, a first slag and steel sampling could be performed with an Al_2O_3 crucible sampler, followed by the introduction of the refractory finger into the melt. Once the scheduled reaction time was reached, the refractory sample was withdrawn from the furnace and quenched with argon gas. Finally, a second sampling of the slag/metal was carried out. To clarify the temperature gradient in the melt and to obtain a better understanding of the temperature influence on slag/refractory interactions, a temperature profile of the crucible with a charge of 15 kg of stainless steel was measured in a separate melting test.[13]

Sample preparation and analysis techniques

Refractories

The recovered cylindrical refractory fingers were sliced into three pieces with a diamond saw: the slag zone sample was used for post-mortem assessment. To evaluate the corrosion behaviour in the different positions along the direction perpendicular to the slag surface, three specimens were prepared from all three slag zone samples. This is demonstrated in Figure 1b: the three sample types consist of the cross section at the top (SH) and the bottom (MH) part of the slag zone, and the vertical section at the bottom of the slag zone (SV). The specimens were embedded in a low viscosity resin (Epofix) by vacuum impregnation, ground with diamond plates, and polished with diamond paste. Finally, carbon was evaporated on the sample surface to provide a conducting layer for microstructural characterization. The polished specimens were assessed with a high resolution SEM (Philips XL-30 FEG), equipped with an EDS detector system (from EDAX) with an ultra-thin window.

Slags

Bulk slag compositions were determined with Inductively Coupled Plasma Atomic Emission Spectroscopy (ICP-AES), using an accurate and precise analysis procedure (dissolution of slags by hot phosphoric acid digestion).[14] Table II shows the as-delivered Al_2O_3-poor VOD slag composition. ICP-AES-analyses of the bulk slag compositions before and after the rotating finger tests revealed similar values as in Table II, albeit with substantially higher Al_2O_3-levels (15–20 mass per cent). Slag layers attached to the refractory specimens were measured with semi-quantitative SEM-EDS analyses (Table III).

Results and discussion

Local corrosion

Figure 2 illustrates that local corrosion occurred at the slag/metal/refractory and, to a lesser extent, at the slag/gas/refractory interface regions. The enhanced attack at the slag/metal/refractory interface was believed to be the result of the combined effect of the strong agitation at the slag/metal interface caused by the metal induction, and the Marangoni convection generated by an interfacial tension gradient.[15] The local corrosion at the slag/metal/refractory interface was expressed through the determination of the maximum local corrosion depth, L_m. The values for L_m were measured microscopically (for Test 1 and 2) and macroscopically (for Test 3) through, respectively, SEM images of vertical section specimens and optical measurements prior to sample preparation. As expected, the maximum local corrosion depth increased with the test duration. For Test 3 (240 min, at 1670°C), L_m reached a value of 5 mm. The local corrosion phenomenon was also observed in the VOD process of a stainless steel company[1] During a 'normal' VOD process, local corrosion does not seem to dominate the refractory lining wear. However, in an exceptional case where the refined liquid melt had to be contained in the ladle for an extended period (5 hours) before being cast, local degradation rings at the slag/metal interface had formed.

Overview of worn microstructures

A general overview of the microstructural features for the hot face specimens at both the top (SH1, SH2 and SH3) and bottom (MH1, MH2 and MH3) slag zone is shown in Figure 3. The corrosion behaviour is characterized by slag infiltration, inactivation of secondary chromite at elevated temperature, and dissolution and decomposition of chromite spinel. The detailed corrosion phenomena are now described for each test run.

Table III
Compositions of slag layer covered on the sample surface after completion of test (mass%), as determined by SEM-EDS

Sample	MgO	Al_2O_3	Cr_2O_3	SiO_2	CaO	FeO
SH1	11.7	17.5	-	34	33	< 0.5
MH1	11.6	17.9	3.6	33	33	0.7
SV1	12.3	19.5	6.1	31	31	< 0.5
SH2	10.4	17.1	3.0	34	33	< 0.5
MH2	12.2	19.1	4.2	34	31	< 0.5
SV2	11.4	17.1	3.2	34	33	< 0.5
SH3	10.4	15.8	4.1	35	34	< 0.5
MH3	11.4	15.8	1.9	37	34	< 0.5
SV3	10.2	18.7	4.2	36	31	< 0.5

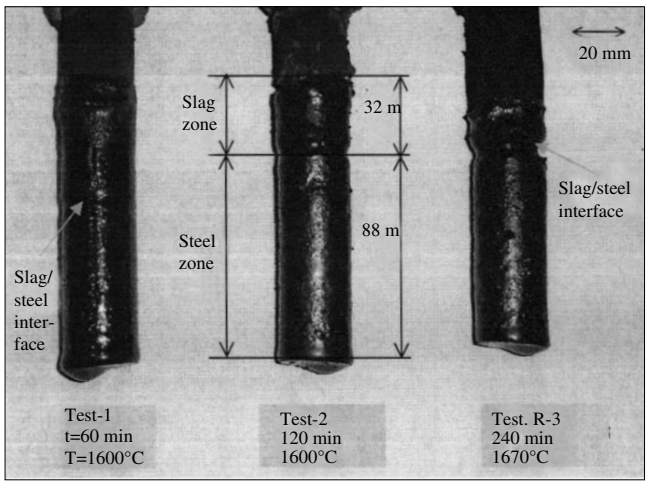

Figure 2. Digital images of the appearance of the worn specimens after tests, showing local corrosion of magnesia-chromite refractory at the slag-metal interface for different experimental conditions

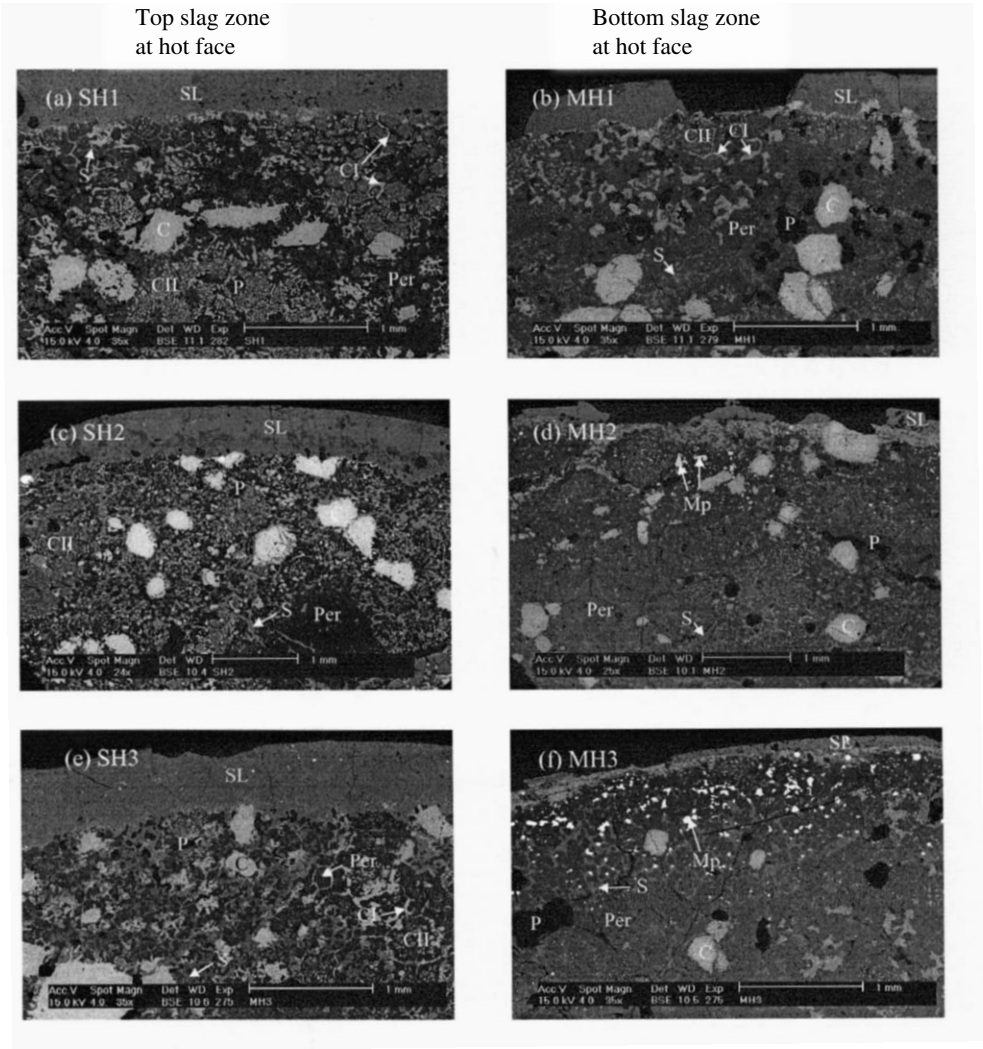

Figure 3. Overview for Tests 1, 2 and 3 of the microstructural features of the hot face at the top (SH 1, 2 and 3) and bottom (MH 1, 2 and 3) slag zone: Per = magnesia (periclase); C = primary chromite; CI = Secondary chromite type I; CII = secondary chromite type II; S = infiltration slag; SL = slag layer; Mp = metallic particle; P = pore or crack

Test 1 (1600°C, 60 min)

Figures 3a and b are Back Scattered Electron (BSE) images of the specimens for Test 1 at, respectively, the top and bottom slag zone. The bottom slag zone sample was completely infiltrated by slag, whereas only a small fraction of slag infiltration was observed in the top slag zone specimen. Accordingly, the brick at the top slag zone remained almost intact: its microstructure seems analogous to that of the as-delivered brick, in which a large amount of secondary chromite was located both at the periclase grain boundaries (Type I) and within these grains (Type II). Contrastingly, there was a substantial decrease in the quantity of secondary chromite phases in the bottom slag zone specimen. This distinct corrosion level observed at different positions is likely to have been caused by the temperature gradient along the refractory sample height, which is discussed in a later section. No FeO_x or Cr_2O_3 decomposition was observed.

Test 2 (1600°C, 120 min)

Figure 3c (top slag zone) and Figure 3d (bottom slag zone) reveal a considerable modification of the microstructure of the corroded samples. The brick was completely infiltrated by slags even at the top slag zone. FeO_x or Cr_2O_3 decomposition occurred in the hot face of the bottom slag zone sample, both in the periclase solid solution (i.e. magnesia containing dissolved FeO_x, Cr_2O_3 and Al_2O_3) and in the chromite spinel phases. No metallic particles were observed at the top slag zone sample. The quantity of secondary chromite was considerably less than it was in Test 1, particularly at the top slag zone. The dissolution of primary chromite into infiltrating slag was observed (Figure 3c).

Test 3 (1670°C, 240 min)

These samples were the most severely degraded, as depicted in Figure 3f (bottom slag zone) and Figure 3e (top slag zone): the infiltrated areas in the interior of refractory finger extended further, while the level of remaining secondary chromite was drastically reduced. In the bottom slag zone it had almost completely disappeared. A substantial number of metallic particles with relatively large sizes was present in the periclase and chromite phases at the refractory surface layer (bottom slag zone). Similarly, as in Test 1 and 2, no FeO_x or Cr_2O_3 decomposition occurred at the top slag zone.

Summary

Some general conclusions can be drawn: (1) no FeO_x or Cr_2O_3 decomposition from the periclase solid solution or

spinel phases occurred at the top slag zone in all three tests, although it was established at the bottom slag zone close to the slag/refractory interface, particularly for the test with the highest temperature and longest time; (2) slag fully penetrated throughout the refractory samples, and the secondary chromite disappeared to a large extent at the bottom slag zone samples; (3) the dissolution of primary chromite into slags was observed in Test 2. The involved refractory wear mechanisms are discussed in the following sections.

Slag infiltration and MgO dissolution

Slag layer

The high Al_2O_3 contents for the present tests were achieved through Al_2O_3 dissolution from the crucible into the slag, prior to the actual finger test experiments. As can be seen in Figure 3, all specimens were covered with a slag layer on their surface, with Al_2O_3 contents ranging from 15 to 20 mass per cent (Table III). Visual observation of these slag layers suggests that there exists an inverse relationship between the experimental temperature and the thickness of the slag layer. This can be explained by the fact that the slag solidification rate is inversely proportional to the slag temperature during cooling. Higher slag viscosity of the slag at lower temperatures is a second reason for this phenomenon.

Effects of corrosion time and temperature

The variation of the slag infiltration in the refractory as a function of time and temperature is demonstrated in Figure 4, indicating that with an increase in holding time and temperature, slag infiltration increases substantially with a simultaneous decrease in the remaining secondary chromite level (Figures 4b and c). The periclase and primary grains were heavily attacked by the infiltrating slag

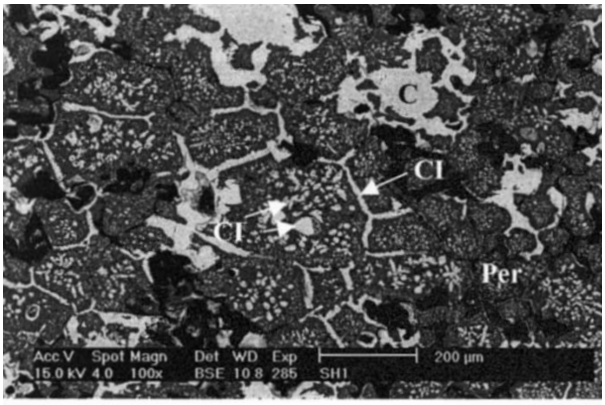

(a) SH1
Time = 60 min
Temp. = 1600°C

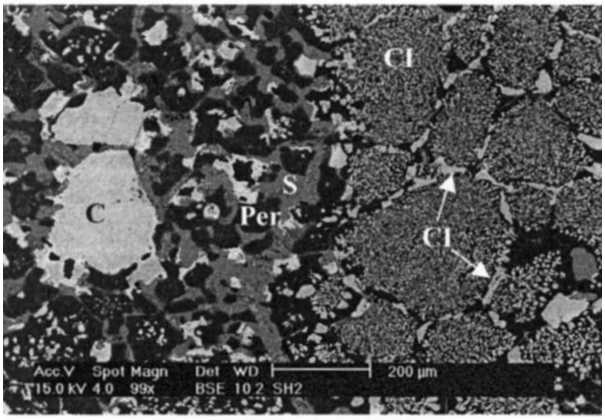

(b) SH2
Time = 120 min
Temp. = 1600°C

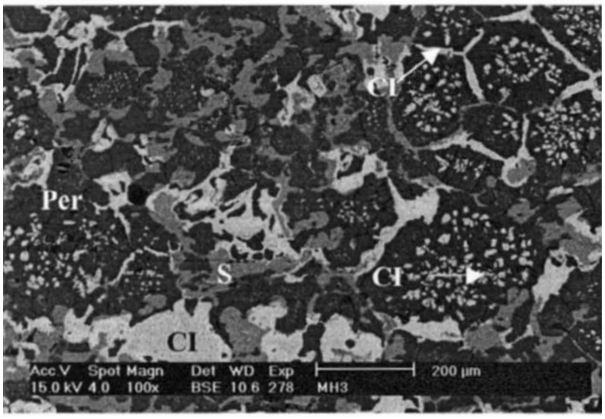

(c) SH3
Time = 240 min
Temp. = 1670°C

Figure 4. BSE images of Test 1, 2 and 3 at top slag zone in center of samples, showing time-dependance of slag infiltration: Per = periclase; S = silicate-slag phase; C = primary chromite; CI = secondary chromite type I; CII = secondary chromite type II

in Tests 2 and 3. As for a given test, the local temperature at the different sample positions (top or bottom slag zone) is the only variable experimental parameter, their distinct corrosion behaviour is believed to be the result of the temperature gradient.

To estimate this gradient in the slag zone, a temperature profile was measured (Figure 5). It becomes evident that the higher experimental temperature leads to a larger temperature gradient in the melt. In the present experimental temperature range, the temperature of the bottom slag zone was confirmed to be more than 100°C higher than that of the top slag zone. Figure 6 shows the distinct slag infiltration for the different sample positions, which is thus believed to be the direct result of the temperature gradient along the slag zone. As can be seen from Figure 6a (top slag zone), slag penetrated into the refractory finger less than 600 µm, whereas at the bottom slag zone (Figure 6b) an infiltrated network of liquid slag was observed even at the sample centre. This infiltration occurs primarily along the periclase grain boundaries. Elevated temperatures enhance slag infiltration due to the decrease in slag viscosity and the disappearance of secondary chromite at higher temperatures.

MgO dissolution into slag

Refractory dissolution in the slag phase inevitably occurs whenever the infiltrating slag is not saturated with certain components (e.g. MgO). This was confirmed in the present experiments by comparing the compositions of the slag layers attached to sample hot faces with those of the infiltrated slag inside the refractory finger. EPMA-EDS analyses revealed that the MgO content of the infiltrated slag is on average 2 mass per cent higher than that of the slag layers on top of the hot face. MgO dissolution into the slag leads to the formation of low melting point compounds that crystallize as $CaO{\cdot}MgO{\cdot}SiO_2$ (CMS) and/or $3CaO{\cdot}MgO{\cdot}2SiO_2$ (C_3MS_2) upon cooling.

Degradation of primary chromite

Two primary chromite degradation mechanisms were clearly observed in this experiment: (1) infiltrated slag dissolves primary chromite grains (Figure 7a), and (2) FeO_x or Cr_2O_3 decomposition occurs at elevated temperatures (Figure 7b). The latter was observed only in the bottom slag zone samples, which implies that temperature strongly affects the decomposition behaviour. In general, the chemical decomposition of FeO_x and Cr_2O_3 can be expressed, respectively, as:

$$FeO\ (s) = Fe(1) + 1/2\ O_2\ (g); \quad \Delta G_3^0 = 287340 - 73.7 * T \qquad [3]$$

$$Cr_2O_3\ (s) = 2Cr(s) + 3/2\ O_2\ (g); \quad \Delta G_4^0 = 1110000 - 247 * T \qquad [4]$$

where ΔG_3^0 and ΔG_4^0 are the standard Gibs free energy changes expressed in J per mole[16] for, respectively, FeO_x (expressed as 'FeO') and Cr_2O_3 decomposition. The FeO_x or Cr_2O_3 decomposition process is determined by the temperature, the oxygen potential and the activities of FeO_x or Cr_2O_3 in primary chromite spinel. Note that this phenomenon also takes place in the periclase solid solution phase. Due to the fact that the activities are predetermined in a given refractory and the oxygen partial pressure was fixed to be 10^{-11} atm, temperature was the only operation variable in the present tests. This explains why the number of metallic particles so strongly depends on the experimental temperature (see Figure 4). The present

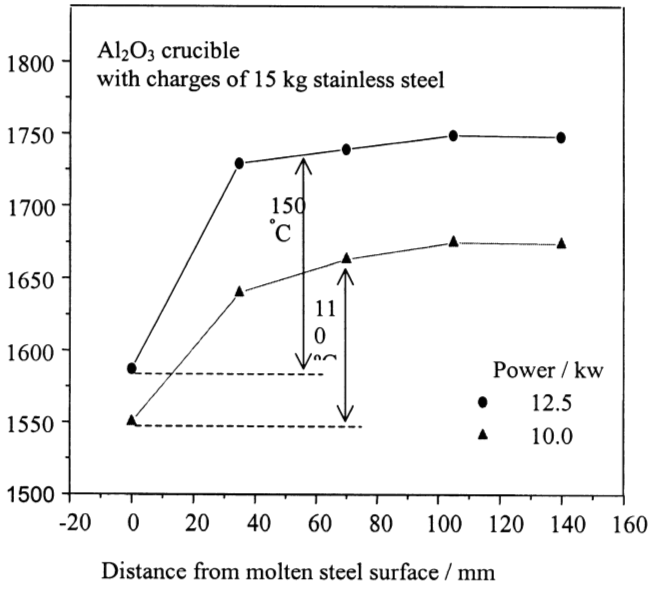

Figure 5. Temperature profile of molten steel bath in the experiments

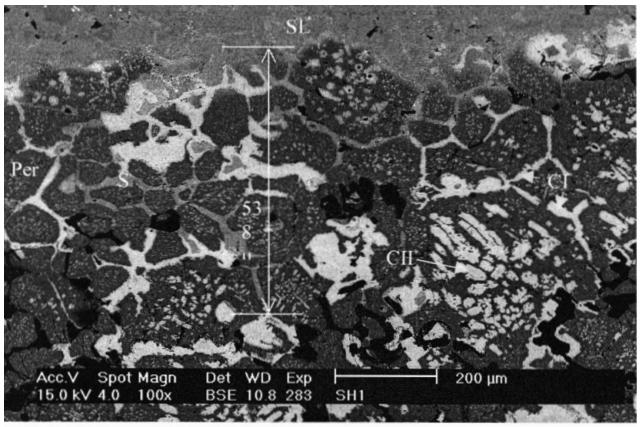

a) Test 1, Top slag zone at hot face

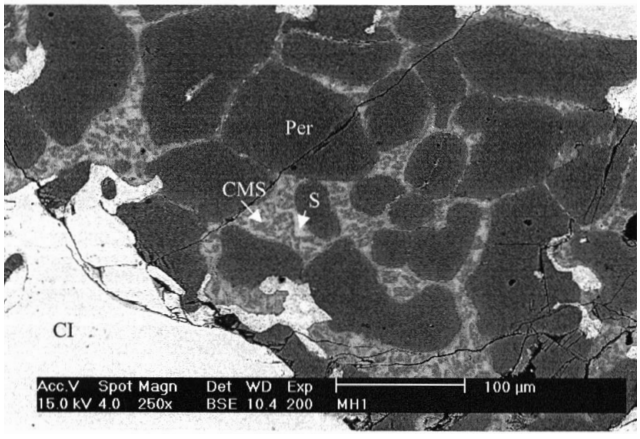

b) Test 1, bottom slag zone at sample centre

Figure 6. BSE images of Test 1 at different positions, showing the temperature influence on the behaviour of slag infiltration: Per = periclase; SL = slag layer; S = infiltrated slag; CI = secondary chromite type I; CII = secondary chromite type II

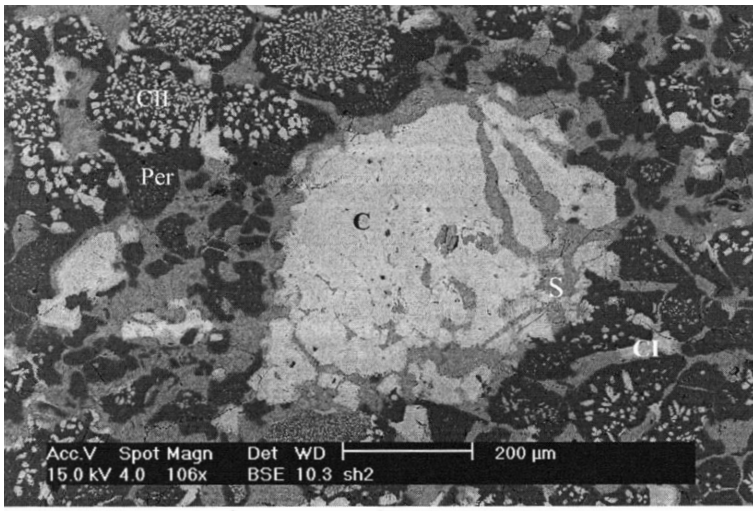

(a) Infiltrated slag attack on primary chromite

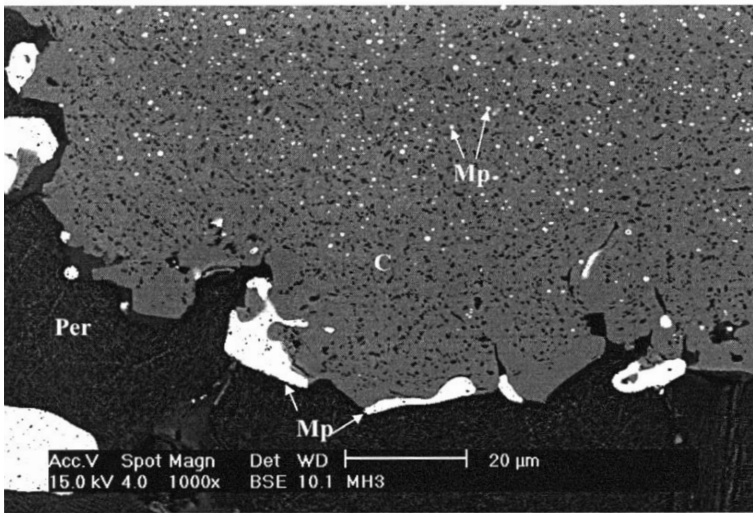

(b) Iron and chromium oxide decomposition from primary chromite

Figure 7. Degradation mechanism of primary chromite, showing (a) Slag attack on primary chromite, and (b) iron and chromium oxide decomposition from primary chromite grains: Per = periclase; S = infiltration slag; CI = secondary chromite type I; CII = secondary chromite type II; C = primary chromite; Mp = metallic particle

results indicate that the decomposition occurs as the temperature is in excess of 1600°C. Figure 8b shows the oxide decomposition process in the primary chromite grains. A substantial number of small metallic droplets (< 1 µm) could be located in the primary chromite matrix. This suggests that, as a result of the low oxygen pressure and the high temperature, the decomposition started from the nucleation of liquid droplets along the cracks and pores in the interior of the chromite crystals, followed by a growth of the droplets with further decomposition. Finally, these droplets merged, forming larger size metal phases. As the decomposition proceeds, a large number of labyrinth-like pores or cracks were formed in the chromite matrix as a result of volumetric shrinkage associated with the decomposition reactions. The shrinking further facilitates both the nucleation of metallic droplets and the removal of oxygen gas (from the reaction site) generated during the decomposition.

Table IV gives an overview of the compositional changes of the primary chromite for distinct levels of decomposition. The presence of metallic particles is associated with a significant decrease in FeO_x content (measured as 'FeO') in the chromite matrix. The metallic droplets resulting from the decomposition of the primary chromite crystals were rich in iron (> 80 mass per cent) with smaller levels of chromium (< 20 mass per cent), indicating that FeO_x decomposition is more predominant than Cr_2O_3 decomposition. This is consistent with the results shown in Table IV (low FeO content in the primary chromite with metallic particles) and previous findings by the present authors[1,3] This enhances further slag infiltration and its reaction with the chromite components, which accelerates the wear of the primary chromite grains.

As regards to the direct dissolution of primary chromite into the infiltrating slag, attention should be paid to the slag compositions. Because of the amphoteric character of Al_2O_3, an increase in the Al_2O_3 level in the present relatively acidic slag (Table III) results in (1) a higher slag basicity (see Equation [2]), thus decreasing the slag resistance of chromite, and (2) a more fluid slag (Al_2O_3 behaves as a network breaker in this case), facilitating slag infiltration. This results in a more elevated primary chromite dissolution. This finding is confirmed by the experiments of Demir and Eric[12] who reported that increasing the Al_2O_3 to CaO ratio of a slag causes an increase in the dissolution rate of chromite.

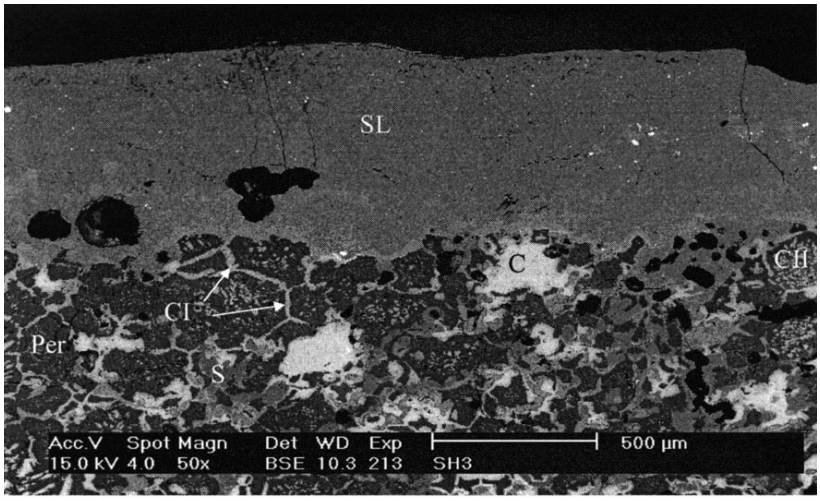

(a) Test 3, top slag zone at hot face

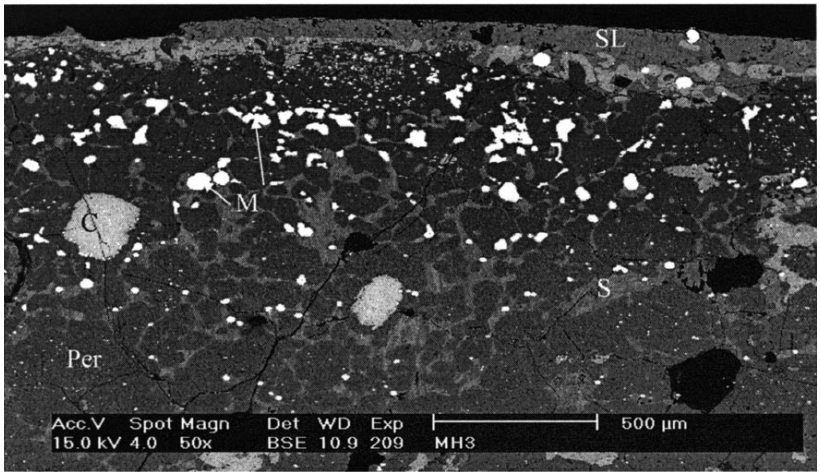

(b) Test 3, bottom slag zone at hot face

Figure 8. Secondary chromite degradation of Test 3 at different postions, showing strong position-dependence (temperature different): Per = periclase; SL = slag layer; S = infiltrated slag; CI = secondary chromite type I; CII = secondary chromite type II; C = primary chromite; Mp = metallic paticle

Table IV
Compositions of primary chromite under different conditions (mass%), as determined by SEM-EDS

Sample	MgO	Al_2O_3	Cr_2O_3	FeO	Note
MH1	20.5	17.0	52	10.5	Without decomposition (no metallic particle in primary chromite)
SH1	18.0	17.5	56	8.8	
SH2	20.1	16.7	51	11.8	
SH3	21.2	17.0	49	12.5	
MH2	20.7	19.2	58	2.0	With decomposition (major presence of metallic particles)
MH3	23.2	17.6	54	5.0	
As-del.*	18.3	15.9	52	11	As-delivered bricks with heating to different temperature and rapid quenching to room temperature
1500°C*	18.0	14.5	53	14	
1600°C*	18.6	15.7	53	12	
1700°C*	17.0	15.0	53	13	

*Data cited from Ref. 1.

High-temperature inactivation of secondary chromite

The degradation behaviour of secondary chromite phases can be understood from Figure 8. A thicker slag layer attached to the top slag zone sample surface (Figure 8a) implies a lower temperature at this position. A substantial amount of secondary chromite phase was still present (after 240 minutes) together with the infiltrated slag in the top slag zone refractory finger, whereas, the secondary chromite almost completely disapperared in the bottom slag zone refractory finger (Figure 8b). A great many metallic particles in both periclase and spinel phases, resulting from FeO_x or Cr_2O_3 decomposition, were scattered in the hot face region close to refractory surface.

Since for a given test, apart from the temperature gradient, there were no changes in the value of experimental parameters in the slag zone, it is inferred that the higher temperature imposed on the bottom slag zone effectively activated the diffusion of the components of secondary chromite into surrounding periclase solid solution and/or its dissolution into the infiltrated slag (see above for the role of high Al_2O_3 levels). This leads to its gradual disappearance in the refractory microstructure.

Apart from some remaining scattered primary chromite crystals, the original two-phase direct-bonded microstructure (periclase + chromite) is thus largely transformed into a much weaker one-phase (periclase solid solution) liquid-bonded structure, which accelerates refractory wear when exposed to turbulent process conditions. This is in agreement with the previous findings of the high temperature inactivation mechanisms of the secondary chromite.[1–2]

Conclusions

In order to simulate refractory wear in Al_2O_3-rich slags for VOD processes, rotating finger tests were performed in a vacuum induction furnace. Cylindrical rebonded magnesia-chromite refractory samples were brought into contact with CSMA slags containing 15 to 20 mass per cent Al_2O_3. The microstructure of the worn samples and their degradation mechanisms were investigated through post-mortem microstructural characterization. The influence of the experimental temperature and the Al_2O_3 content of the slag on the slag/refractory interactions were discussed. The following conclusions could be drawn:

- Local corrosion was observed at both the slag/metal/refractory and the gas/slag/refractory interface, particularly in the test with the longest and hottest exposure conditions. The slag/metal/refractory local corrosion was predominant. It is thought to be the combined effect of Marangoni flows and agitation at the slag/metal interface caused by steel induction.
- When comparing the top and bottom slag zones of the respective samples, severe degradation was noticed in the latter, while the former were less corroded. The main reason for this is the vertical temperature gradient along the sample (with a higher temperature in the bottom slag zone).
- Slag infiltrates the refractory finger through the open pore network and along the periclase grain boundaries. The infiltration increases with corrosion time and temperature. High temperature inactivation of secondary chromite phases enhances this process.
- Primary chromite degradation occurs according to two distinct mechanisms: FeO and Cr_2O_3 decomposition and dissolution by infiltrated slag. The former occurs because of low oxygen potentials and high temperatures, whereas the latter is probably enhanced by the high Al_2O_3 content of the slag. During decomposition, small metallic particles and pores are generated, which form homogenously in the interior of the primary chromite matrix. The pores are believed to be the result of volumetric shrinkage during the decomposition reaction.
- FeO_x and Cr_2O_3 decomposition may also proceed in the periclase solid solution phase, if temperatures are in excess of 1600°C. This results in a further destabilization of the refractory hot face, possibly inducing peeling and/or spalling mechanisms.[1,3]
- The present tests suggest that high Al_2O_3 contents in relatively acidic VOD slags presumably lead to a poorer slag resistance of chromite spinel in magnesia-chromite refractories with reference to Al_2O_3-poor VOD slags.[1,3] However, further investigation is required to evaluate the influence of the Al_2O_3 content in the slag on the degradation of periclase and the possibility to induce passive corrosion through the formation of a dense $MgO.Al_2O_3$ spinel layer that can prevent major slag infiltration.
- Finally, it was shown that the present experimental procedure is an excellent tool for the in-depth study and simulation of refractory degradation mechanisms in industrial metallurgical processes, allowing one to diminish the risks associated with industrial plant trials.

Acknowledgements

This work was performed with the financial and technical support of U&A Belgium and the IWT (project no. 990348). The authors are grateful to the engineers of U&A Belgium and PVA for their close co-operation with our team. Practical advice from Heraeus Electro-Nite and the University of Gent was much appreciated.

References

1. JONES, P.T. Degradation Mechanisms of Basic Refractory materials during the Secondary Refining of Stainless Steel in VOD Ladles, Ph.D. Thesis, Acco (Leuven), 2000.
2. JONES, P.T., VLEUGELS, J., VOLDERS, I., BLANPAIN, B., VAN DER BIEST, O., and WOLLANTS, P.A Study of Slag-infiltrated Magnesia-chromite Refractories using Hybrid Microwave Heating. *Journal of the European Ceramic Society*, vol. 22. 2002. pp. 903–916.
3. JONES, P.T, BLANPAIN, B., WOLLANTS, P., DING, R., and HALLEMANS, B. Degradation Mechanisms of magnesia-chromite refractories in VOD ladles and measures to extend the lining life. *Ironmaking and Steelmaking*, vol. 27, no. 3. 2000. pp. 228–273.
4. MOSSER, J., BUCHEBNER, G., and DÖSINGER, K. New high-quality MgO-Cr_2O_3-bricks and Cr-free alternatives for the lining of RH/DH-vessel. *Veitsch-Radex Rundshau*, no. 1. 1997. pp. 33–39.
5. CALKINS, D.J., GILBERT, V., and SACCOMANO, J.M. Refractory wear in the argon-oxygen-decarburization process. *Ceramic Bulletin*, vol. 52. 1973. pp. 570–574.
6. NARITA, K., ONOYE, T., SATOH, Y., and TANIKCHI, K. Slag testing of refactories for ladle refining by ESR method. *Taikabutsu* (Refractory), vol. 36. 1984. pp. 273–277.
7. WHITWORTH, D.A., JACKSON, F.D., and PATRICK, R.F. Fused basic refractories in the argon-oxygen-decarburization process. *Ceramic Bulletin*, vol. 53. 1974. pp. 804–808.
8. TAKAHASHI, H., KAWAKAMI, T., OGUCHI, Y., and TSUCHIYA, I. Application of high Cr_2O_3 magnesia chrome refractories to secondary refining

systems. *Taikabutsu* (Refractory), vol. 40. 1988. pp. 564–566.

9. KYODEN, H., ICHIKAWA, K., and IWADO, H. Texture and slag resistance of commercial fused magnesia-chrome clinker. *Taikabutsu* (Refractory), vol. 37. 1985. pp. 284–290.

10. ENGEL, R., MARR, R., and PRETORIUS, E. Refractory/slag system for ladles and secondary refining processes. *Iron and Steelmaker*, vol. 24, no. 4. 1997. pp. 59–60.

11. LEONARD, R.J. and HERRON R.H. Volume expansion and structural damage in periclase-chrome refractories. *Ceramic Bulletin*, vol. 51. 1972. pp. 891–895.

12. DEMIR, O. and ERIC, R.H. Dissolution of Chromite in Liquid Slag: Empirical Relationship. *Proceedings 6th International Conference on Molten Slags, Fluxes and Salts*. Stockholm, 2000.

13. GUO, M., DYCK, J.V., PARADA, S., JONES, P.T., BLANPAIN, B. and WOLLANTS, P. Laboratory Induction Furnace to Study Refractory Materials Degradation in a Controlled Atmosphere at High Temperature. *ATB-Metallurgie*, 2003. in print.

14. JONES, P.T., HERMANS, P., BLANPAIN, B., and WOLLANTS P. Optimization of an Accurate and Precise Analysis Procedure for Metallurgical VOD Slags With ICP-OES. *Atomic Spectroscopy*, 21. 2000. pp. 86–92.

15. TAO, Z., MUKAI, K., and OGATA, M. Local Corrosion of Magnesia-Chromite Refractory at Slag-Metal Interface. *Taikabutsu Overseas*, vol. 19. 1999. pp. 3–10.

16. ENGH, T.A. *Principles of Metal refining*, Oxford, Oxford University Press, 1992. pp. 407–425.